Soft Matter

Accepted Manuscript

ROYAL SOCIETY OF CHEMISTRY

www.rsc.org/softmatter

ARTICLE TYPE www. rsc.org/xxxxxx | XXXXXXXX

Static lengths in glass-forming monodisperse hard-sphere fluids from periodic array pinning

Yuxing Zhou and Scott T. Milner*

Received Xth XXXXXXXXXX 20XX, Accepted Xth XXXXXXXXX 20XX
First published on the web Xth XXXXXXXXXX 200X
DOI: 10.1039/b000000x

We explore the static length in glass-forming hard-sphere liquids revealed by the response of dynamical properties (diffusion coefficient D and α relaxation time τ_α) to a regular array of pinned particles. By assuming a universal scaling form, we find data can be excellently collapsed onto a master curve, from which relative length scales can be extracted. By exploiting a crystal-avoiding simulation method that suppresses crystallization while preserving dynamics, we can study monodisperse as well as polydisperse systems. The static length obtained from dynamical property Q (τ_α and D) scales as $\log Q \sim \xi_s^{\psi}$, with $\psi \approx 1$.

1 Introduction

The origin of sluggish motions in supercooled liquids is still a matter of debate. Under the general view of cooperative motion in glass-forming liquids, growing (or diverging) relaxation times should be associated with one or more growing (or diverging) length scales.

On the one hand, a dynamic correlation length, characterizing the growth of spatially heterogeneous dynamics as temperature decreases, can be extracted from multipoint space-time correlation functions[1,2]. This correlation length depends on the delay time, and reaches its peak value near the alpha relaxation time τ_α. However, although the relaxation time and dynamic length both grow as the temperature decreases, it has been suggested they might not be directly related[3]. The question remains unsettled, whether dynamic heterogeneity is the origin or only a consequence of glassy dynamics.

On the other hand, many efforts have been made to identify a "hidden" static length responsible for the slow dynamics. Since it is difficult to identify any amorphous order parameter from the apparently unchanged structure during glass formation, static lengths are often computed either from spatial correlations of some *a priori* local order, such as icosahedrons[4], polytetrahedrons[5] or medium-range crystalline order[6], or by an "order-agnostic" approach, including the point-to-set (PTS) technique[7] and excess plastic modes analysis[8]. It is unclear whether static lengths estimated by different approaches agree with each other.

One of the most studied static lengths is the PTS length ξ_{ps}. A general procedure[7,9–11] of obtaining ξ_{ps}, motivated by random first-order transition (RFOT) theory, is as follows. All particles in an equilibrated system outside of a spherical region of radius R are frozen, while the inner particles are allowed to relax in the presence of the frozen boundary. The RFOT theory predicts that for $R \gg \xi_{ps}$, the subsystem inside the cavity should decorrelate from its initial state in favor of configurational entropy; whereas for $R \ll \xi_{ps}$, the subsystem is trapped into the initial state due to the cost of surface tension (mismatch on the boundary). To measure whether the subsystem of radius R can eventually switch to a different state, the long time limit of an global overlap function $Q_\infty(R)$ is introduced. The PTS length is defined as the radius for which $Q_\infty(\xi_{ps})$ falls below some small value.

Although defined by *static* overlap, the PTS length might be generally regarded as the characteristic length over which the fixed boundary conditions imposed by pinning particles affect the *dynamics* of nearby particles. This interpretation suggests that we can reveal the static length from the response of some dynamical property (such as the particle self-diffusion coefficient) to an imposed pinning field.

In several recent works, the effect of pinned particles on structural relaxation has been studied in systems with soft potentials[12–15]. To extract a correlation length, these authors have made different theoretically motivated assumptions for how the structural relaxation time τ_α depends on pinning strength, such as $\tau_\alpha \sim \exp(Ac)$ with c the pinning concentration[12,14] or $\ln \tau_\alpha \sim \exp(Bz)$ with z the distance from the wall[13,15].

There is some variation in recent glass literature in how the terms "static" and "dynamic" length are used. In Refs. 13 and 15, correlation lengths obtained by this approach are called "dynamic", although they are not obtained from multipoint space-time correlation functions, to distinguish them from the "static" PTS length extracted from analysis of overlap at long times in the presence of pinning. In this work, we obtain a

Department of Chemical Engineering, Pennsylvania State University, University Park, State College, PA, 16803, USA. E-mail: stm9@psu.edu; Fax: +1-814-865-7846; Tel: +1- 814-863-9355

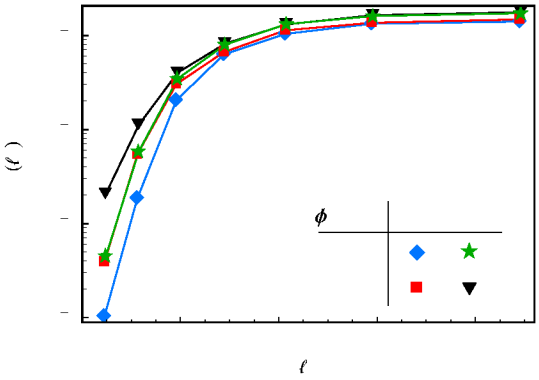

Fig. 1 Confining length dependence of diffusivity for monodisperse and polydisperse systems (at $\phi = 0.56$), for periodic array and random pinning.

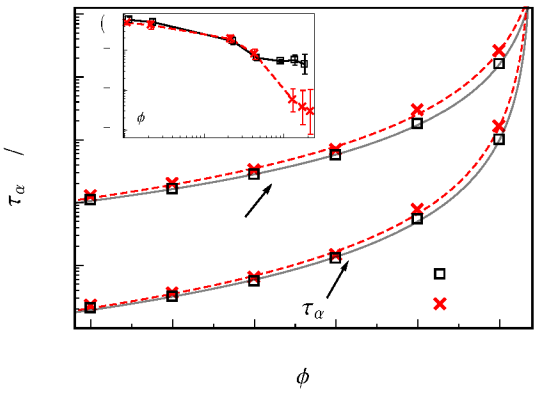

Fig. 2 Self-diffusion coefficient D and alpha relaxation time τ_α as a function of ϕ for monodisperse and polydisperse system ($s = 0.08$). Dashed and solid lines are MCT fits. Inset: aging of diffusion coefficient D at $\phi = 0.59$ as a function of equilibration time τ_e .

length scale by analyzing the effect of pinning on dynamical properties (self-diffusion coefficient and structural relaxation time). Although our length scales are obtained from the response of dynamical properties to pinning, we follow the earlier usage and call these lengths "static", to emphasize that they are not obtained from multipoint correlation functions and do not depend on a choice of time delay.

In this work, we use molecular dynamics (MD) simulation of monodisperse hard-sphere systems to learn how dynamical properties change as the pinning length scale varies, and extract static correlation lengths from scaling analysis without assuming a specific functional form. Two typical dynamical properties are examined in this work, namely the diffusion coefficient D and alpha relaxation time τ_α.

2 Method

The hard-sphere fluid is the simplest system that exhibits a glass transition, at a volume fraction $\phi_g \approx 0.59$[16,17]. In experiments on colloidal hard-sphere suspensions, particles can be pinned using optical tweezers[18]. To avoid crystallization above the freezing point $\phi_f \approx 0.495$, a moderate polydispersity in particle size s is usually introduced. However, polydispersity does alter the dynamics, especially in the vicinity of glass transition. For polydisperse hard spheres at high ϕ, small particles may remain diffusive while large ones are almost arrested, so that the ideal monodisperse glass transition is smeared out[19].

To avoid this artifact, we exploit a crystal-avoiding (CA) hybrid Monte Carlo method that suppresses crystallization in monodisperse hard spheres while preserving the dynamics[20]. Although pinning some particles tends to frustrate crystallization, we find that the monodisperse hard-sphere system still crystallizes readily at low pinning fraction ($c < 6\%$). To prevent crystallization and to be consistent across different pinning fractions, we employ the CA method for all simulations reported here.

Results are reported in standard hard-sphere units: mean sphere diameter σ, mean sphere mass m and temperature $k_B T$ are taken to be unity.

3 Results

While random pinning has been proposed as the best candidate for studying static correlation[21], we focus here on periodic array pinning, in which particles nearest to the corresponding nodes of a $m \times m \times m$ grid are pinned, so that the pinning fraction is $c = m^3/N$. The confining length ℓ_c is then defined as $\ell_c = L/m$, with L the system size. In this way, ℓ_c is unaffected by variations that may arise by random pinning, as a result of fluctuations in the locations of pinned particles. Array pinning also avoids spatial heterogeneity induced by randomly pinned particles, that may mimic intrinsic dynamical heterogeneity. Some modified random pinning schemes[22,23] have been used for similar purposes.

Fig. 1 compares the effect of pinning on diffusivity for monodisperse and polydisperse systems with array and random pinning at $\phi = 0.56$, as an example. It is evident that fluctuations in both particle sizes (polydispersity) and pinned particle positions (random pinning) diminish the liquid-glass transition.

We consider hard-sphere systems of $N = 2000$ particles for ϕ ranging from 0.53 to 0.58. For each ϕ, initial configurations are generated using the Lubachevsky-Stillinger algorithm and then equilibrated. For unpinned monodisperse systems, we calculate the self-diffusion coefficient D (extracted from the long-time limit of mean square displacement (MSD)) and al-

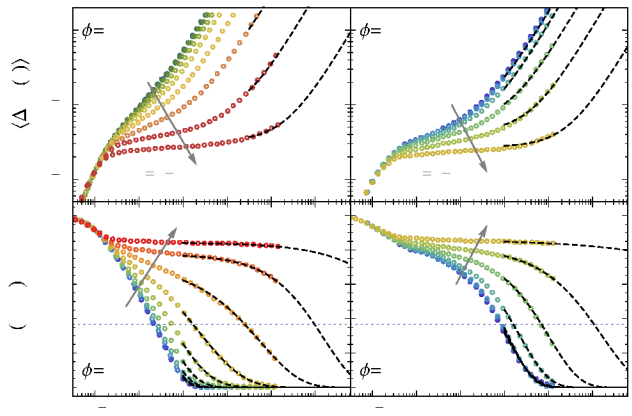

Fig. 3 Pinning effect on mean-squared displacement $\langle \Delta r^2(t) \rangle$ and intermediate scattering function $F_s(q_0,t)$ for monodisperse systems at $\phi = 0.53$ and $\phi = 0.57$. The confining length ℓ_c ranges from infinity down to 1.39σ for $\phi = 0.53$, and from infinity down to 2.04σ for $\phi = 0.57$. Dashed lines are fits described in main text.

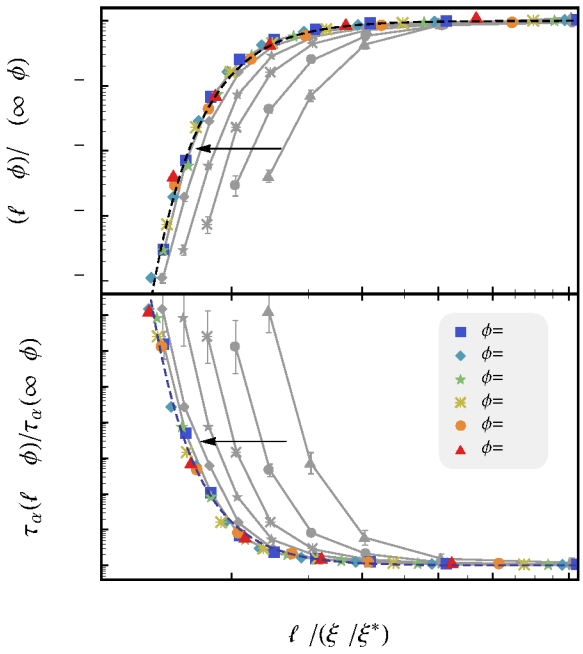

Fig. 4 Normalized diffusion coefficient $D(\ell_c,\phi)/D(\infty,\phi)$ and α relaxation time $\tau_\alpha(\ell_c,\phi)/\tau_\alpha(\infty,\phi)$, for different ϕ and confining length ℓ_c. Raw data with error bars (one standard error) are in gray. Dashed lines are guides for the eye.

pha relaxation time τ_α (defined as the time at which the intermediate incoherent scattering function $F_s(q,\tau_\alpha)$ equals $1/e$, with $q = 6.5$ near the first peak in $S(q)$), and compare to results for polydisperse systems (see Fig. 2).

The dramatic increases in both $1/D$ and τ_α are well described by a power-law divergence,

$$1/D \text{ or } \tau_\alpha \sim (\phi_c - \phi)^{-\gamma}, \qquad (1)$$

inspired by mode-coupling theory (MCT). We fit the data $\log 1/D$ and $\log \tau_\alpha$ versus ϕ to Eq. (1) using standard nonlinear regression and find that for monodisperse systems, $\phi_c = 0.586 \pm 0.003$, $\gamma = 2.5 \pm 0.5$ for $1/D$ and $\phi_c = 0.584 \pm 0.002$, $\gamma = 2.6 \pm 0.4$ for τ_α. For our polydisperse system ($s = 0.08$), we have $\phi_c = 0.586 \pm 0.001$, $\gamma = 2.2 \pm 0.1$ for $1/D$ and $\phi_c = 0.584 \pm 0.001$, $\gamma = 2.4 \pm 0.2$ for τ_α. Although the MCT calculation for hard-sphere systems using the Percus-Yevick approximation gives a much smaller $\phi_{c,\mathrm{MCT}} \approx 0.52$[24], ϕ_c obtained here agrees well with the experimental glass transition in colloidal suspensions, $\phi_g \approx 0.59$.[16,17]

Alternatively, the same data can be equally well fit by an Voge-Fulcher-Tammann (VFT)-like form

$$1/D \text{ or } \tau_\alpha \sim \exp\left[A/(\phi_0 - \phi)\right]. \qquad (2)$$

with $\phi_0 = 0.605 \pm 0.006$ for $1/D$ and $\phi_0 = 0.599 \pm 0.002$ for τ_α for the monodisperse system, and $\phi_0 = 0.604 \pm 0.002$ for $1/D$ and $\phi_0 = 0.599 \pm 0.001$ for τ_α for our polydisperse system. Although the dynamics appears barely altered by small polydispersity when the system is far from glass transition, strong aging is observed at $\phi = 0.59$ in monodisperse systems (Fig. 2 inset); in contrast, aging in polydisperse systems at $\phi = 0.59$ is much less pronounced, because of the decoupling of dynamics of small and large particles[19]. As we shall see below, the glass transition can also be induced by pinning particles even at $\phi \ll \phi_g$, hence polydispersity should be expected to affect dynamics under pinning whenever the system becomes glassy. Indeed, we observe a weaker pinning effect on dynamics for polydisperse systems (see Fig. 1).

To expose a static length using pinning, an array of particles are frozen in an equilibrated configuration, while the remaining unpinned particles are allowed to move. For each ϕ, we vary the number of pinned particles m^3 from zero up to the value at which the system is essentially frozen during the simulation. The confining length is related to m as $\ell_c/\sigma = \left(\frac{\pi N}{6\phi}\right)^{1/3}/m$. For each ϕ and m, MSD and $F_s(q_0,t)$ are averaged over five independent initial configurations, with at least five realizations of array pinning for each initial configuration. Up to 10 pinning realizations are used at higher ϕ and higher pinning fraction, where run-to-run fluctuations in MSD and structural relaxation function become larger. (Since the center of mass of unpinned particles can diffuse due to collisions with pinned particles, all particle positions are calculated with respect to the mean position of the unpinned particles.)

Fig. 3 illustrates the pinning effect on MSD and $F_s(t)$ for $\phi = 0.53$ and $\phi = 0.57$. The array of pinned particles evi-

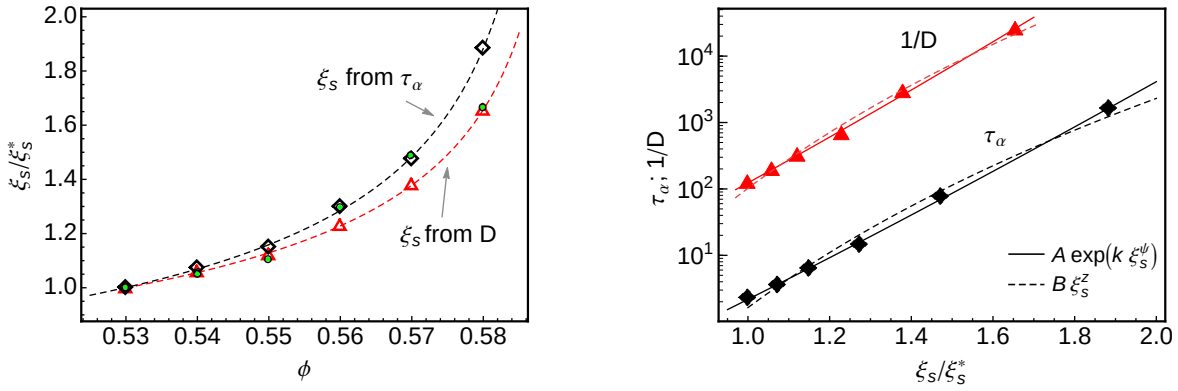

Fig. 5 (a) Static lengths obtained from master curve construction of diffusion coefficient (triangles) and alpha relaxation time (diamonds) as a function of ϕ; dashed lines are power law fits. Also included are "Kauzmann" critical lengths (disks) extracted from fitting inspired by RFOT theory[29]. (b) D and τ_α versus the static length ξ_s obtained from the corresponding quantity, with ξ_s^* at $\phi = 0.53$ used as reference.

dently hinder the motions of unpinned particles — the growth of $\langle \Delta r^2(t) \rangle$ and decay of $F_s(t)$ become slower with increasing m or decreasing ℓ_c. Moreover, the pinning effect is more pronounced in the more dense system — a smaller value of m is sufficient to freeze the system — consistent with an increasing static length scale. In other words, the glass transition can also be induced by pinning particles in a dense liquid with $\phi < \phi_g$ or $T > T_g$, which opens a new way to study the glass transition[25].

At high pinning concentration, our simulation time is unavoidably limited compared to the slow relaxation time. Nonetheless, we can estimate the diffusion coefficient D from the slope of a linear plot of MSD versus time assuming the diffusive region has been reached. Likewise, we can obtain the the alpha relaxation time τ_α as the $1/e$ time of $F_s(q_0,t)$ with the final decay fit to a stretched exponential. Since the configuration of unpinned particles is automatically in equilibrium after pinning[22,26], the measured MSD and $F_s(q_0,t)$ are correct equilibrium values, i.e., they do not show aging; and the accuracy of estimated D and τ_α is only limited by the simulation time. In fact, our values for D and τ_α are reasonably robust, in that we find since no significant change in our results when we use longer runs at selected state points.

Having obtained D and τ_α for an array of values for ϕ and confining length ℓ_c, we can extract static lengths ξ_s from a dynamic scaling assumption. For $\ell_c \gg \xi_s$, unpinned particles can barely "feel" the presence of pinned particles, and dynamic properties are governed by the static correlation length ξ_s. As ℓ_c decreases and becomes comparable to ξ_s, the dynamics crosses over from being governed by ξ_s to ℓ_c.

Assuming this crossover behavior depends only on the ratio of characteristic lengths ℓ_c/ξ_s, a given dynamic property Q at different ϕ and ℓ_c can be described by a scaling form

$$\frac{Q(\ell_c;\phi)}{Q(\infty;\phi)} = f\left(\frac{\ell_c}{\xi_s(\phi)}\right), \qquad (3)$$

in which Q is either $1/D$ or τ_α, and $f(x)$ is a dimensionless scaling function. A master curve can be constructed by horizontally shifting the curves of $Q(\ell_c;\phi)/Q(\infty;\phi)$ plotted versus $\log \ell_c$. Up to an overall prefactor, the static length $\xi_s(\phi)$ for each ϕ can be determined from the corresponding shift factor.

To construct the master curve without knowing the form of $f(x)$, we define the "smoothness" of a given set of n points as the arc length of its linear interpolation curve. A better collapse of our data (Fig. 4) with fewer twists and turns result in a smaller arc length. The master curve is obtained by horizontally shifting raw data points and numerically minimizing the arc length with respect to the shift factors, with $\phi_0 = 0.53$ taken as reference and left unshifted. (See Appendix for details.)

As shown in Fig. 4, normalized data for both D and τ_α collapse onto smooth master curves that span nearly four decades for diffusion coefficients and six decades for α relaxation time, confirming our scaling assumption (Eq. 3). An analogous data collapse τ_α versus system size $N^{1/3}$ has been previously reported in systems without pinning, using the static length obtained from the minimum eigenvalue of the Hessian matrix[27]. However, because of the rather weak dependence of τ_α on system size, the range of τ spans less than one decade. We find that the diffusion coefficient and relaxation time become decoupled as the pinning concentration increases, consistent with recent reports[28]. Despite this behavior (related to the breakdown of the Stokes-Einstein relation, see below), we find that the scaling form Eq. 3 describes both the diffusion coefficients and relaxation times very well (see Fig. 4).

Based on RFOT theory and renormalization group method,

Ref. 29 predicts τ_α with random pinning scales as $\log\tau \sim 1/(c_K - c)$ for high $T > T_K$, where c is the pinning concentration and c_K the "Kauzmann" concentration at which the configurational entropy S_c vanishes. If we fit the raw data for τ_α at different ϕ to this form and extract the static length as $\xi_s = (\rho c_K)^{-1/3}$, the results are in line with those from our master curve construction (see Fig. 5). However, it is difficult to obtain robust values for ξ_s by this procedure, since the fitting parameters are so sensitive that we must exclude certain data at high pinning fractions to get reasonable values (see SM). In contrast, the master curve covers a wider range of data and is more robust.

As can be seen in Fig. 5(a), the static length ξ_s grows mildly by a factor of two or so over the range of ϕ accessible to our simulations, comparable with previous observations in a wide variety of systems [10,30–32]. Our results can be well fit by a power law,

$$\xi_s \sim (\phi_s - \phi)^{-\nu}, \quad (4)$$

yielding $\phi_s = 0.593 \pm 0.001$, $\nu = 0.32 \pm 0.01$ for D; and $\phi_s = 0.589 \pm 0.001$, $\nu = 0.34 \pm 0.01$ for τ_α. Although the values for ϕ_s are slightly larger than our results for ϕ_c obtained from fitting the divergences in D and τ_α, they agree within statistical error. To see the relation between the static length and dynamics, we plot $1/D$ and τ_α versus ξ_s in Fig. 5 (b). The results can be fit either by a power-law form, $Q \sim \xi_s^z$, or by an activated scaling behavior, $\log Q \sim k\xi_s^\psi$, yielding $z = 10.6 \pm 0.6$, $\psi = 1.2 \pm 0.3$ for $1/D$ and $z = 10.5 \pm 0.7$, $\psi = 1.2 \pm 0.2$ for τ_α.

Within the RFOT theory, scaling relations of the form $\log\tau_\alpha \sim \xi_s^\psi$ and $\xi_s \sim (1/S_c)^{1/(d-\theta)}$ are expected, where S_c is the configurational entropy and d is the space dimension. While $\psi \approx 1$ is generally quoted which agrees with our result, the value of exponent θ is controversial, varying from 0.3 to 2.3. [33–35]. Nevertheless, by assuming the Kauzmann volume fraction $\phi_K \sim \phi_s$ and $S_c \sim (\phi_K - \phi)^\beta$, with $\beta = 0.30 \pm 0.04$ approximated from a law-power fit of the $S_c(\phi)$ data in Ref. 36 (which also gives $\phi(S_c = 0) \approx 0.587 \sim \phi_s$), we estimate $\theta \approx 2.1$ for hard-sphere systems.

We note that the ξ_s obtained from D grows more slowly than the length obtained from τ_α, suggestive of the decoupling of $1/D$ and τ_α with increasing ϕ (see Fig. 2), signaling the breakdown of the Stokes-Einstein relation. Since this breakdown can be qualitatively understood as the consequence of dynamic heterogeneity — D is dominated by the mobile particles while τ_α results from the immobile ones — the difference between ξ_s from D and ξ_s from τ_α may also arise from differently weighted averages of a spectrum of static lengths present in the system [7]. Despite the growing discrepancy between $1/D$ and τ_α and their corresponding ξ_s, the proportionality constants k in the relations $\log 1/D \sim k\xi_s$ and $\log\tau_\alpha \sim k\xi_s$ are nearly identical (assuming the two static length scales coincide at low ϕ).

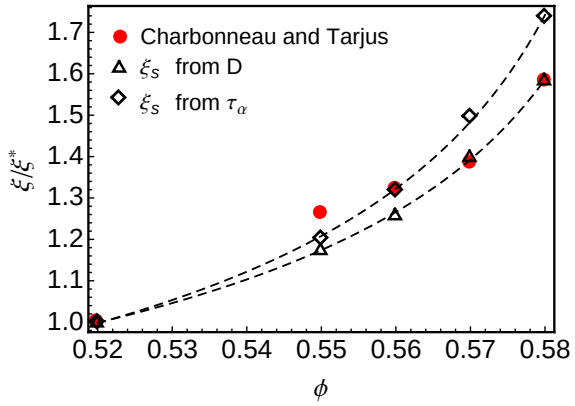

Fig. 6 Comparison of static lengths obtained from scaling and master curves, and PTS lengths from configurational overlap. Static lengths are normalized by their values at $\phi = 0.52$.

We have also applied our methods to bidisperse particles, and compare the static lengths obtained from our scaling and master curves to PTS lengths obtained from configurational overlap. Following Ref. 30, we randomly pinned an equimolar binary mixture of N=2000 particles with a diameter ratio 6:5. We perform standard event-driven MD for ϕ=0.52,0.55,0.56,0.57 and 0.58 and check that the pressures and diffusion coefficients are consistent with those reported in Ref. 30. The resulting static lengths is shown in Fig. 6 as a function of ϕ, which agree reasonably well with the PTS lengths previously reported. [30]

4 Summary

To conclude, we present a simple way of extracting static lengths based on the response of dynamic properties to an external pinning field. By exploiting a recently developed crystal-avoiding method, we simulate the monodisperse hard-sphere metastable fluids and calculate D and τ_α in the presence of a periodic array of frozen particles. (We use a periodic array (here simple cubic) to minimize local heterogeneity induced by random pinning locations; however, we expect that other lattices or even pinning sites with liquidlike correlations would behave similarly.) We find a universal scaling description of dynamic crossover as a function of confining length ℓ_c over the range of ϕ studied. A master curve is constructed by optimizing its "smoothness", from which we extract static lengths ξ_s for both D and τ_α, which grow moderately with increasing ϕ as the dynamics slows dramatically. The two ξ_s obtained for D and τ_α decouple at higher ϕ, suggesting a distribution of static lengths in different regions of the system. Scaling relations between dynamical quantities and the static lengths of the form $\tau_\alpha \sim \exp(k\xi_s^\psi)$ and $\xi_s \sim (\phi_s - \phi)^{1/(d-\theta)}$

with $\psi \approx 1$ and $\theta \approx 2$ are consistent with RFOT, but investigations at higher ϕ are needed for more precise values. It would be interesting to apply our method to systems with soft potentials, and compare the results to static lengths obtained by other methods.

Appendix

Here we depict how to obtain the shift factor for data collapse (see Fig. 4) using arc-length minimization. In Fig. 7(a) and (b), we exemplify our method by horizontally shifting the data for normalized τ_α versus $\log \ell_c$ at $\phi = 0.55$, while fixing the data for $\phi = 0.53$ as a reference. As we vary the shift, the "smoothness" of the resulting linear interpolation curve changes. In general, we find smaller arc length of the interpolation corresponds to better data collapse; the optimal shift factor is obtained when the arc length is minimized. The same method applies when more than two curves are shifted simultaneously, in which case the minimization is conducted over multiple shift factors.

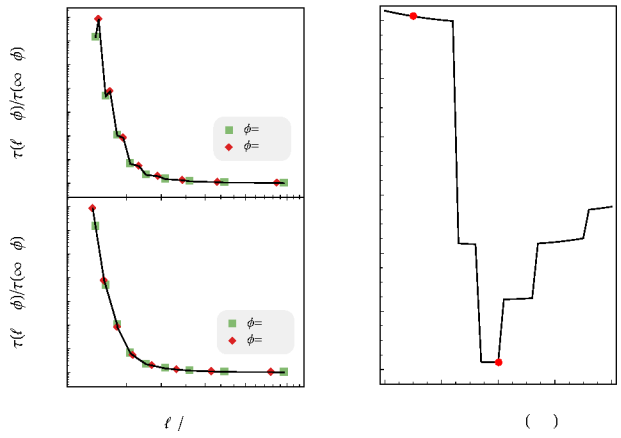

Fig. 7 An illustration of finding the shift factor that minimizes the arc length of linear interpolation of the data. Left: data collapse for two different shift factors. Right: arc length versus shift factor, with corresponding shift factors in (a) and (b) marked.

References

1 L. Berthier, G. Biroli, J.-P. Bouchaud, L. Cipelletti, D. El Masri, D. L'Hôte, F. Ladieu and M. Pierno, *Science*, 2005, **310**, 1797–1800.
2 E. Flenner, M. Zhang and G. Szamel, *Phys. Rev. E*, 2011, **83**, 051501.
3 S. Karmakar, C. Dasgupta and S. Sastry, *Proceedings of the National Academy of Sciences*, 2009, **106**, 3675–3679.
4 M. Dzugutov, S. Simdyankin and F. Zetterling, *Phys. Rev. Lett.*, 2002, **89**, 195701.
5 A. Anikeenko and N. Medvedev, *Phys. Rev. Lett.*, 2007, **98**, 235504.
6 T. Kawasaki, T. Araki and H. Tanaka, *Phys. Rev. Lett.*, 2007, **99**, 215701.
7 J.-P. Bouchaud and G. Biroli, *J. Chem. Phys.*, 2004, **121**, 7347.
8 S. Karmakar, E. Lerner and I. Procaccia, *Physica A*, 2012, **391**, 1001–1008.
9 G. Biroli, J.-P. Bouchaud, A. Cavagna, T. S. Grigera and P. Verrocchio, *Nat Phys*, 2008, **4**, 771–775.
10 G. M. Hocky, T. E. Markland and D. R. Reichman, *Phys. Rev. Lett.*, 2012, **108**, 225506.
11 A. Cavagna, T. Grigera and P. Verrocchio, *Phys. Rev. Lett.*, 2007, **98**, 187801.
12 K. Kim, *EPL*, 2003, **61**, 790–795.
13 W. Kob and D. Coslovich, *Phys. Rev. E*, 2014, **90**, 052305–7.
14 S. Chakrabarty, S. Karmakar and C. Dasgupta, *Sci. Rep.*, 2015, **5**, 12577.
15 Y.-W. Li, W.-S. Xu and Z.-Y. Sun, *Journal of Chemical Physics*, 2014, **140**, 124502.
16 P. N. Pusey, E. Zaccarelli, C. Valeriani, E. Sanz, W. C. K. Poon and M. E. Cates, *Phil. Trans. R. Soc. A*, 2009, **367**, 4993–5011.
17 G. Brambilla, D. El Masri, M. Pierno, L. Berthier, L. Cipelletti, G. Petekidis and A. B. Schofield, *Phys. Rev. Lett.*, 2009, **102**, 085703.
18 S. Gokhale, K. H. Nagamanasa, R. Ganapathy and A. K. Sood, *Nat Commun*, 2014, **5**, 4685.
19 E. Zaccarelli, S. M. Liddle and W. C. K. Poon, *Soft Matter*, 2015, **11**, 324–330.
20 Y. Zhou and S. T. Milner, *Soft Matter*, 2015, **11**, 2700–2705.
21 L. Berthier and W. Kob, *Phys. Rev. E*, 2012, **85**, 011102.
22 W. Kob and L. Berthier, *Phys. Rev. Lett.*, 2013, **110**, 245702.
23 G. M. Hocky, L. Berthier and D. R. Reichman, *Journal of Chemical Physics*, 2014, **141**, 224503–9.
24 T. Franosch, M. Fuchs, W. Gotze, M. R. Mayr and A. P. Singh, *Phys. Rev. E*, 1997, **55**, 7153–7176.
25 S. Karmakar and G. Parisi, *PNAS*, 2013, **110**, 2752–2757.
26 P. Scheidler, W. Kob, K. Binder and G. Parisi, *Philosophical Magazine Part B*, 2009, **82**, 283–290.
27 S. Karmakar and I. Procaccia, *Phys. Rev. E*, 2012, **86**, 061502.
28 Y.-W. Li, Y.-L. Zhu and Z.-Y. Sun, *Journal of Chemical Physics*, 2015, **142**, 124507–10.
29 C. Cammarota and G. Biroli, *PNAS*, 2012, **109**, 8850–8855.
30 P. Charbonneau and G. Tarjus, *Phys. Rev. E*, 2013, **87**, 042305.
31 A. J. Dunleavy, K. Wiesner, R. Yamamoto and C. P. Royall, *Nat Commun*, 2015, **6**, 6089.
32 G. Biroli, S. Karmakar and I. Procaccia, *Phys. Rev. Lett.*, 2013, **111**, 165701.
33 C. Cammarota, A. Cavagna, G. Gradenigo, T. S. Grigera and P. Verrocchio, *J. Chem. Phys.*, 2009, **131**, 194901.
34 T. R. Kirkpatrick, D. Thirumalai and P. G. Wolynes, *Phys. Rev. A*, 1989, **40**, 1045–1054.
35 S. Sastry, F. W. Starr and J. F. Douglas, *J. Chem. Phys.*, 2013, **138**, 12A541.
36 L. Angelani and G. Foffi, *J. Phys.: Condens. Matter*, 2007, **19**, 256207.

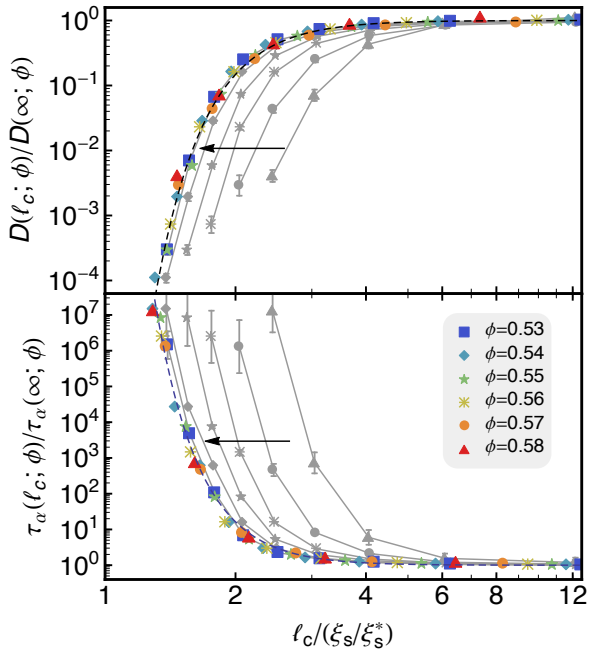

In glassy hard-sphere fluids, with varying particle volume fraction and distance between pinned particles, particle diffusivities and structural relaxation times both collapse to master curves, revealing a growing static length scale.